

Dynamical models of a suspension bridge driven by vibration data

Vincenzo Gattulli^{*1}, Alvaro Cunha^{2a}, Elsa Caetano^{2b},
Francesco Potenza^{3c}, Andrea Arena^{1d} and Umberto Di Sabatino^{4e}

¹ Department of Structural and Geotechnical Engineering, Sapienza University of Rome, Via Eudossiana 18, 00184 Rome, Italy

² Construct-ViBest, Faculty of Engineering (FEUP), University of Porto, Rua Dr. Roberto Frias, 4200-465 Porto, Portugal

³ Department of Engineering and Geology, University G. d'Annunzio of Chieti-Pescara, Viale Pindaro 42, 65127 Pescara, Italy

⁴ Department of Civil, Construction-Architectural and Environmental Engineering, University of L'Aquila, Piazzale E. Pontieri 2, 67100 L'Aquila, Italy

(Received November 20, 2020, Revised December 12, 2020, Accepted December 16, 2020)

Abstract. The great availability of measurement systems permits to acquire quite easily data related to structural oscillations in operational conditions. This occurrence may permit to enhance our capability to data-driven computing using directly experimental data and pertinent constraints and conservation laws, such as compatibility and equilibrium, surely certain. In the paper, a methodology will be presented to furnish an analytical mechanical model of a suspension bridge in which the main parameters can be derived from vibration measurements. In this respect, Polymax and Enhanced Frequency Domain Decomposition identification procedures are used to determine a complete modal model which is used to evaluate an error function. Optimization algorithms are used to evaluate the function minima in the fundamental parameter space. The procedure will be validated by results coming from a sophisticated finite element model for which geometric measurements are included through a 3D point cloud geometrical model and a consequent Building Information model (BIM) constructed with images acquired by unmanned aerial vehicle (UAV). The case study of the pedestrian cable suspension Polvorines bridge (100 meters of span) is considered to demonstrate the procedure, due the test campaign conducted on March 2020.

Keywords: vibration measurements; polymax; model updating; error optimization; modal identification

1. Introduction

Among the most important typologies of bridges able to cover long span the ones realized by suspension cable or cable-stayed are very used worldwide. Anyway, the whole process of construction is highly expensive but these structures will go to constitute a valuable asset for the countries, institutions or companies responsible of the management. Due to their long expected service life, they could be subjected to severe dynamics loads, like earthquakes or typhoons. Moreover, strong attention should be paid on the effects induced by environmental parameters (fluctuations of humidity and temperature) like materials deterioration (e.g., corrosion). Lastly, also the consequences of cyclic loads (fatigue) could have a remarkable impact on the structural behavior changes. For these reasons, such structures should be maintained in good conditions guaranteeing an opportune level of performance able to comply both serviceability and safety requirements.

Structural Health Monitoring (SHM) and Experimental Modal Analysis (EMA) constitute two of the most prominent tools used to obtain useful information related to the assessment of the structural health. In the last decades, many efforts have been devoted to the design, implementation and manage of the structural health monitoring systems for Suspension Bridges (SBs). In Siringoringo and Fujino (2018), it is described the permanent system installed on the Hakucho Suspension Bridge from 1998 to 2006 to monitor the seismic response. It was composed by 27 channels of accelerometers that have been able to record the response induced by different earthquakes with various amplitude allowing to define a relationship between the identified frequencies and amplitude ground motion. In Caetano *et al.* (2018) and Hu *et al.* (2012) is highlighted the importance of a continuous dynamic monitoring system along the whole life cycle of the structure (design, construction, commissioning, service or rehabilitation phase). In the latter contest, among the different tasks to be pursued, can be underlined: check of the serviceability safety, evaluation of the traffic loads and wind effects and damage detection. In Koo *et al.* (2013) a multi-component instrumentation (temperature and wind sensors, strain gauges, displacement sensors) system has been used to carry out the structural health monitoring of Tamar Bridge, a hybrid of cable stay and suspension bridge. In this case study large differences on the identified modal frequencies have been found with the temperature changes. Others scientific papers regarding the SHM for SBs can be

*Corresponding author, Full Professor,
E-mail: vincenzo.gattulli@uniroma1.it

^a Full Professor, E-mail: acunha@fe.up.pt

^b Associate Professor, E-mail: ecaetano@fe.up.pt

^c Assistant Professor, E-mail: francesco.potenza@unich.it

^d Assistant Professor, E-mail: andrea.arena@uniroma1.it

^e Research Fellow, E-mail: umbertodisabatino@virgilio.it

found in Wickramasinghe *et al.* (2020), Mao *et al.* (2017) and Zhou *et al.* (2013).

EMA are, in general, easier to be performed but, since they run for a limited number of days, they are able to provide less information than the ones obtained by SHM. They aimed to identified the main modal features (frequencies, shapes and damping ratios) that characterize the dynamics of the observed structures. In recent years, the vibrations-based methods applied to measurements recorded under environmental noise, easily executable, have been the ones mostly exploited even if the obtained results produce a modal basis that needs to be orthonormalised (Antonacci *et al.* 2012). In Hua *et al.* (2020), the results of a series of tunnel tests on the main cable in construction have been used to develop countermeasures to eliminate harmful wind-induced vibrations. Indeed, in Gattulli *et al.* (2019a), the modal information has been considered to update an analytical model able to interpret the dissipative properties by non-proportional damping.

In general, model-based methods are more suitable for applying the information coming from the data processing of EMA. They use analytical or finite element models to describe as much as possible the experimental evidences. However, even if an accurate updating brings to an optimized model, a characterization of the uncertainties is necessary. For this reason, in the recent years and especially in the case of SHM, model-free methods have been developed to explore the internal characteristics of the raw measured response used for damage detection indices (Nie *et al.* 2020).

In the literature different authors have analyzed the effects of the cable-structures interactions due to various types of actions (Larsen and Larose 2015, Gattulli *et al.* 2019b and 2016). In Gattulli and Lepidi (2007) have been deeply analyzed the spectral properties of stayed-structures through a simple cable-stayed beam model identifying the flipping between local/global (cable/beam) modal shapes within the veering regions. In Caetano *et al.* (2000) and (2008), three-dimensional refined finite element models, representative of the structural dynamic of the Gadiana cable-stayed bridge, have been updated based on experimental data. Moreover, such models have been used to provide possible interpretation of experimental observations related to cable-deck dynamic interaction mechanisms. Other studies are devoted to crowd-structure interaction to describe the changes of the modal features of footbridges in lateral direction as illustrated in Jimenez-Alonso *et al.* (2019).

The present paper aims to investigate the dynamics of suspension cable bridges using the opportunity of taking into account experimental data coming from a large campaign of EMA. A model-based method, able to be enriched by experimental data, is followed to derive a reliable representation of the dynamic behavior of the pedestrian suspended Polvorines bridge in Toledo. The updating of both a synthetic analytical model and a large numerical model of the suspension bridge, has evidenced the complex interaction between main cables and deck even in the linear field for low-amplitude oscillations. The paper is organized as follows: in Section 1 is presented an

analytical mechanical model for suspension bridge, in Section 2 is described the extensive experimental campaign and the results of the data processing, in Section 3 methods used to update both analytical and finite element models are described together with the obtained results.

2. Analytical mechanical model of a suspension bridge

The mechanical model of the suspension bridge here proposed (Fig. 1) to identify the significant mechanical parameters able to represent the measured system dynamics, is based on a novel parametric continuum formulation of the models proposed in Arena and Lacarbonara (2012), Casalotti *et al.* (2014), and Arena *et al.* (2016). The equations describing the free dynamics of the bridge are obtained via a Lagrangian formulation in which the three-dimensional kinematics of the bridge deck and the cables were linearized about the equilibrium configuration under self-weight. Therefore, the cables are subjected to the stress due to dead loads and the initial, horizontal component of the cables tension, here denoted by H , is evaluated from the sag f_0 of the cables in the in-service configuration. The suspension hangers are here assumed to be rigid and modelled as uniformly distributed along the span of the bridge, therefore, such constraint implies that the cables vertical displacement is equal to the deck vertical deflection of the hanger connection points. In the context of small kinematics, the bridge deck dynamics in the axial direction can be neglected since it is characterized by higher frequencies with respect to the vertical and lateral motions. Moreover, the cables spanwise dynamics are neglected, and a static condensation is enforced.

The most straightforward description of the equations governing the free oscillations of the suspension bridge can be obtained by identifying the lowest number of independent mechanical parameters of the system. To this end, the parametric form of the equations of motion is derived by nondimensionalizing the kinematic variables and the mechanical parameters by using a geometric and a time

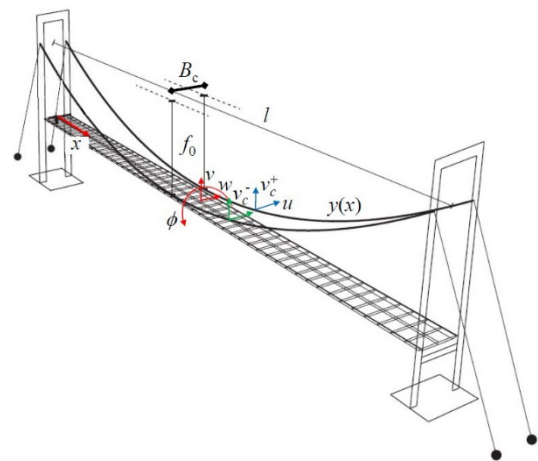


Fig. 1 Schematic 3D view of a suspension bridge mechanical model

characteristic parameter. In particular, the bridge span l and the frequency $\omega_c = \sqrt{EJ_v/(m_D l^4)}$ are taken as characteristic length and frequency, respectively, where EJ_v is the deck flexural stiffness and m_D is the deck mass per unit length. It is worth to mention that the characteristic frequency is calculated a priori for given, tentative, values of EJ_v and m_D , respectively, and it will not change during the simulations, together with the bridge span length l which is also a constant parameter.

Thus, the nondimensional kinematic unknowns of the system are given as their ratio to the bridge span and are the vertical and lateral displacements v and w of the deck centerline, and the cables lateral displacement u , respectively. Finally, the deck torsional rotation ϕ completes the set of kinematic unknowns; the latter, are all functions of the nondimensional spanwise coordinate x , which vary in the nondimensional domain $[0,1]$, and depend on the nondimensional time t , respectively. On the other hand, the geometry of the system is described by the half-distance $B_c/2$ between the suspension cables scaled by the bridge span, that is, by the parameter, $\delta = B_c/(2l)$. Therefore, the linearized expression of the vertical displacement v_c^\pm of each cable can be calculated as: $v_c^\pm = v \pm \delta\phi$, where the plus and the minus discriminate the two cables. Finally, the cables are assumed to be unstretchable under the effect of their own weight, therefore, their reference equilibrium shape is described by the catenary configuration whose derivation is provided in [Irvine] and that, in nondimensional form, can be written as

$$y(x) = \frac{1}{\gamma} \left[\cosh \gamma \left(\frac{1}{2} - x \right) - \cosh \frac{\gamma}{2} \right] \quad (1)$$

where $\gamma = \frac{(m_c + \frac{m_D}{2})gl}{H}$ is the ratio between the total weight suspended by each cable (i.e., here accounting for the weight of a single cable and half the weight of the deck) and the horizontal component H of the cable tension, with g being the gravity acceleration, and m_c the mass per unit length of each cable. The parameter γ can be directly calculated for a given geometry of the cable under dead loads; in particular, from Eq. (1), once the ratio f_0/l between the sag and the span is assigned, γ can be calculated by solving numerically the transcendental equation given by $y(1/2) = -f_0/l$;

Furthermore, the stiffnesses are scaled as follows

$$\begin{aligned} \kappa_v &= \frac{EJ_v}{(m_D \omega_c^2 l^4)}, & \kappa_w &= \frac{EJ_w}{(m_D \omega_c^2 l^4)}, \\ \kappa_\phi &= \frac{GJ_\phi}{(m_D \omega_c^2 l^4)}, & \kappa_c &= \frac{EA_c l^2}{(m_D \omega_c^2 l^4)} \end{aligned} \quad (2)$$

where EJ_v and EJ_w are the vertical and lateral deck bending stiffness, respectively, GJ_ϕ is the deck torsional stiffness, and EA_c is the cables axial stiffness. On the other hand, $\mu = m_c/m_D$ is the ratio between the cable and the deck mass per unit length, while $J_\mu = J_m/(m_D l^2)$ is the nondimensional rotational mass of the deck. Finally, the nondimensional expression of the horizontal component of

the cable tension H can be written as: $\beta = (\mu + 1/2)g/(\gamma \omega_c^2 l)$.

Thus, the system of partial differential equations (PDEs) describing the free oscillations of the suspension bridge can be written in nondimensional form as

$$\begin{aligned} \left(1 + 2 \frac{\mu}{\cos \theta}\right) \ddot{v} + \kappa_v v'''' - 2\beta v'' \\ - \frac{2\kappa_c}{\eta_c} y'' \int_0^1 y' v' dx = 0 \end{aligned} \quad (3)$$

$$\begin{aligned} \left(J_\mu + 2 \frac{\mu \delta^2}{\cos \theta}\right) \ddot{\phi} - (\kappa_\phi + 2\beta \delta^2) \phi'' \\ - \frac{2\kappa_c \delta^2}{\eta_c} y'' \int_0^1 y' \phi' dx = 0 \end{aligned} \quad (4)$$

$$\ddot{w} + \kappa_w w'''' = 0 \quad (5)$$

$$\frac{\mu}{\cos \theta} \ddot{u} - \beta u'' = 0 \quad (6)$$

together with the following boundary conditions $v(0) = v(1) = 0$, $v''(0) = v''(1) = 0$, $\phi(0) = \phi(1) = 0$, $w(0) = w(1) = 0$, $w''(0) = w''(1) = 0$ and $u(0) = u(1) = 0$.

In Eqs. (3)-(6) the prime and the dot indicate partial differentiation with respect to the nondimensional space and time coordinates x and t , respectively, while $\cos \theta = 1/\sqrt{1 + (y')^2}$ and the parameter η_c has the following expression

$$\eta_c = \int_0^1 \left(\sqrt{1 + (y')^2} \right)^3 \quad (7)$$

It is worth noting that, due to the presence of the suspension cables, the linearization of the equations of motion about the equilibrium under self-weight entails the coupling between the dynamics of the vertical and torsional motions of the bridge, while the lateral motions of the deck and the cables are independent.

The Galerkin projection of the PDEs describing the dynamics of the suspension bridge is performed by adopting the lowest n mode shapes of a beam subjected to the same boundary conditions of the bridge deck and of the cables, respectively. To this end, the kinematic unknowns are approximated as

$$\begin{aligned} v &\approx \sum_{i=1}^n q_{v,i}(t) \psi_{v,i}(x), & w &\approx \sum_{i=1}^n q_{w,i}(t) \psi_{w,i}(x), \\ \phi &\approx \sum_{i=1}^n q_{\phi,i}(t) \psi_{\phi,i}(x), & u &\approx \sum_{i=1}^n q_{u,i}(t) \psi_{u,i}(x), \end{aligned}$$

where the trial functions $\psi_{*,i}(x)$ are the mode shapes of the equivalent beam and of the cables, and $q_{*,i}(t)$ are the lagrangian coordinates. The projection into the basis of trial functions $\psi_{*,i}(x)$ of the equations of motion, together with the minimization of the residual of the projected system of equations, allows to reduce the PDEs to a set of linear ordinary differential equations (ODEs). Due to the boundary conditions to which are subjected the unknown

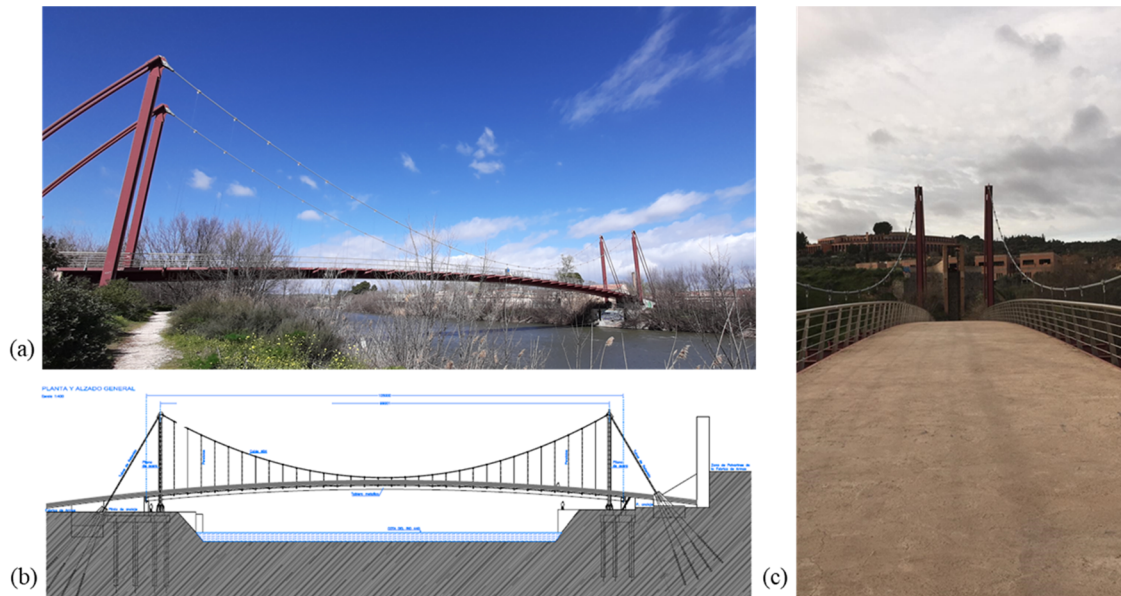


Fig. 2 General view of Polvorines bridge: (a), (b) lateral, (c) longitudinal

variables of the problem here formulated, the trial functions are all the same and corresponds to the trigonometric function $\psi_{*,i}(x) = \sin(i\pi x)$. Finally, the solution of the homogenous ODEs system, in terms of its eigenvalues and eigenvectors, provides the natural frequencies and the mode shapes of the suspension bridge, respectively.

3. Description of the bridge and dynamic tests

The Polvorines walkway (Fig. 2) is a suspension bridge over the Tagus river in the city of Toledo (Spain). Before its construction there was another connecting bridge, still suspension, with a trellis panel, which was however destroyed following a flood in 1947. The actual infrastructure links from a side, north-east, the University Campus of Castilla-La Mancha and from the other one the south-west part of the city. It was opened to cycle and pedestrian traffic in 2007. The bridge was designed by Estudio AIA and constructed by FCC Fomento de Construcciones y Contratas, being made with a mixed steel-concrete system.

The width of the pedestrian crossing is 6 m, while the lateral distance between the two piers is 9 m. The two parallel cables have a sag of 14 m. The 20 m vertical columns, made of steel and hinged at the base, are back-stayed with pairs of circular hollow tubes $\Phi 219 \times 20$.

The transversal structural section of the deck (Fig. 3(a)) is composed mainly by a rectangular box section that runs over the entire length of the deck whose size are of 2 m and 0.762 m, respectively for width and height. Inside this box section, at the bottom and in corresponding of one third and two thirds of the width, have been welded two stiffening elements having a reverse “U” transverse section on the whole length of the deck. Moreover, two additional and important stiffening beam elements have been linked laterally to the transverse section (Fig. 3(c)), one for each side. Such elements have a double “T” transverse section

with a height slightly variable decreasing from the connection to the main section (0.490 m) up to the end of the beam (0.240 m). Just to the end of each beam the hangers have been linked that have the important task of transferring the loads from the deck to the main cables. Such stiffening lateral beams together to the hangers constitute a system that have been disposed each 3 m and so, considering the entire length of the bridge, the total number of the beam-hanger-systems is equal to 32. The lateral beams have also the function to support and distribute the weight of the floor composite slab. This latter is composed by a corrugated sheet and a concrete slab with a total height of about 0.2 m on which is posed a light concrete layer with a thickness of 0.02 m. It is right to highlight that the longitudinal profile of the deck shows a curved variation with a maximum height at the centerline (see Fig. 2(b)). The height difference between the centerline and the end support sections of the deck is of about 2 m. Along the walkway two metal railings have been inserted laterally to protect the pedestrians. They could give a contribute especially related to the rotational inertia of the torsional modes. The diameter of the suspension cable is 84 mm while the one for the hangers is 16 mm. The connection of the main cable at the top of the pylon is made by a hinge as well visible from the photo reported in Fig. 3(f).

A complete list of the mechanical features related to the transversal sections of the main cables and hangers are reported in the Table 1. An interesting detail is related to the realization of the structural supports of the deck visible in the photos inserted in the Figs. 3(d) and 3(e). The first regards only a side of the deck but the same arrangement has been implemented also in the opposite side. The transverse end beams of the deck aim at unloading part of the weight through two equal supports highlighted in the Fig. 3(c). It is evident that, based on this type of system, the only displacements and rotations to be considered locked are the out of plane transversal displacement and torsional rotation. The other four displacements and rotations, i.e., the longitudinal and vertical displacements and the two flexural

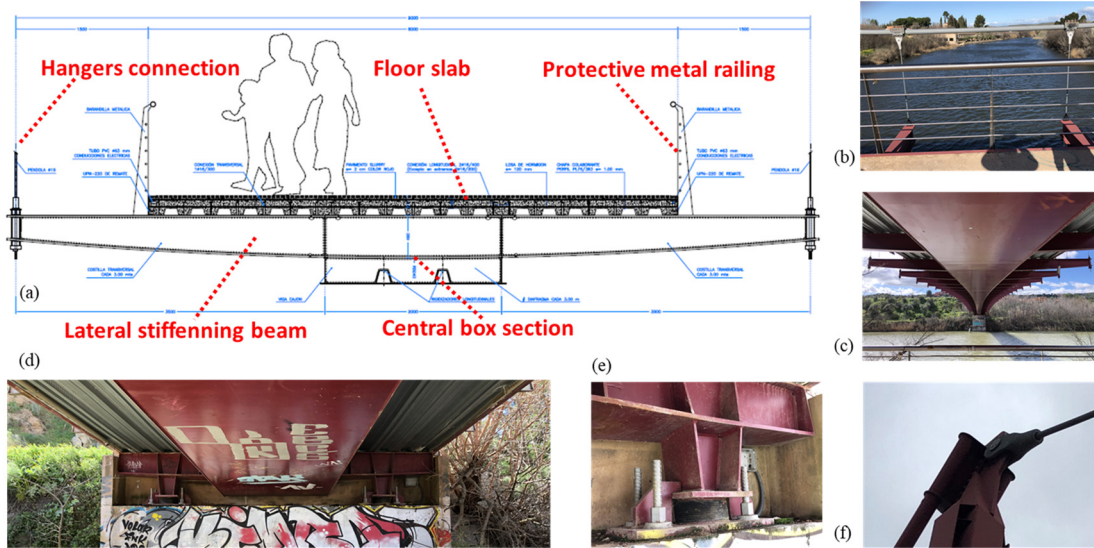
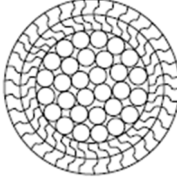


Fig. 3 (a) Transverse section of the Polvorines bridge. (b)-(f) Photos of Polvorines bridge

Table 1 Characteristics of hangers and main cables

Cable	Section	Features	Cable	Section	Features
Hanger		d [mm]: 16	Main		d [mm]: 84
		A [mm ²]: 157			A [mm ²]: 4805
		f _u [kN]: 240			f _u [kN]: 7045
		EA [MN]: 25.9			EA [MN]: 783
		w [kg/m]: 1.3			w [kg/m]: 39.6

d: diameter, A: Area, f_u: ultimate tensile strength, EA: axial stiffness, w: weight per unit of length

rotations, are allowed according to the stiffness of the two rubber (neoprene) supports.

3.1 Experimental instrumentation

The experimental dynamic tests have been carried out on the first week of March, from 02/03/2020 to 05/03/2020. The measurements have been recorded under environmental noise, mainly in the morning. The weather conditions have been characterized by the presence of strong wind. Indeed, has been recorded an average wind velocity of 34.60 km/h with a maximum peak of 48 km/h.

Two types of instrumentation have been used and each of them has been employed to set up different experimental layouts. The first one following:

- (1) Acquisition system: LMS SCADAS XS and Smart Scope.
- (2) 6 Piezoelectric uniaxial accelerometers (PCB 393B31)
- (3) Complementary instrumentation.

Another different typology of instrumentation is composed by 6 independent seismographs (Figs. 4(c) and 4(d)).

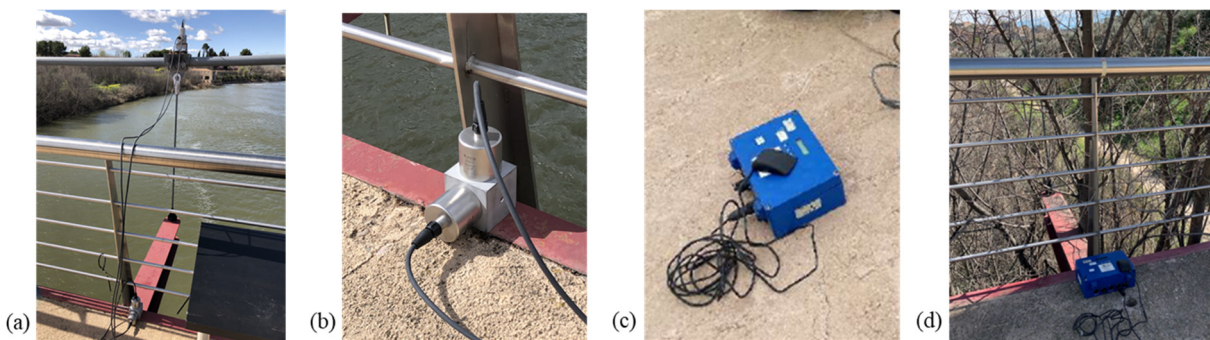


Fig. 4 (a), (b) Photos of the piezoelectric accelerometers mounted on both deck and cables (c), (d); photo of the seismographs

Each of these devices contains a tri-axial accelerometer, as well as a data acquisition and recording system and a GPS antenna. After appropriate programming of the seismographs using a laptop this GPS antenna enables that the several seismographs to make simultaneous measurements without the need of electrical cable.

LMS SCADAS XS is the core of the data acquisition system (first instrumentation) and thanks to its portability and easy use, it is very efficient to maximize the performance of the dynamic tests. It is very suitable for both field and laboratory tests. The important features to be highlighted are the following: (1) the board, can be contained in one hand and, moreover, it is provided of built-in battery; (2) it can have three different modes of operation: wi-fi (connected to Smart Scope), standalone and Front-end; (3) it can support 12 analog channels. The Smart Scope is substantially a tablet on which the user can set up, control and manage the measurement template and but also carry out on-line data processing. The most relevant parameters to be set up are: sensor name, point ID and point direction, typology of the physic quantity to be recorded and its unit of measure, sensitivity, acquisition sample rate.

Table 2 Features of the PCB 393B31 accelerometer

Sensitivity ($\pm 5\%$)	10.0 V/g	Broadband resolution	0.000001 g rms
Measurement range	0.5 g pk	Non-Linearity	$\leq 1\%$
Frequency range ($\pm 5\%$)	0.1 to 200 Hz	Transverse sensitivity	$\leq 5\%$
Resonant frequency	≥ 700 Hz	Overload limit (Shock)	± 40 g pk

Piezoelectric accelerometers have been largely used by a lot of researchers and practitioners operating in the civil engineering field. The sensor showed good performance in the capturing and providing structural information even with a very low vibration amplitude level. The model used here is the PCB 393B31 realized with ICP technology that requires only an inexpensive, constant-current signal conditioner to operate. Its main characteristics are reported in Table 2. The complementary instrumentation is composed, mainly, by the different typologies of coaxial cables needed for both transmissions of the measured data and power supply. In particular, two cables (coaxial cable RG 178/179, custom-cable 052BR010AC), from a side, have to be linked to the board LMS SCADAS and to the piezoelectric sensor, respectively, while the third cable (coaxial cable RG58) have to be linked in the other free end of the two previous cables (it has only extension function). Moreover, to better obtain a good link between the sensor and structure has been realized a customized aluminum cube with a central thread for screw insertion, in each face, to connect the accelerometric sensor (Fig. 4(b)). Furthermore, in one of the six cube faces have been introduced four magnetic elements for a rapid and ease connection in steel or iron structure points. A special connection has been used to link the sensors with the cable (Fig. 4(a)). The mounting of the sensors on the cables have been possible thanks to the support of climbers.

3.2 Experimental setups

The experimental layouts have been opportunely designed to identify the main frequencies, modal shapes and modal damping factors associated to the primary system (deck) and cables. One of the targets is also to investigate

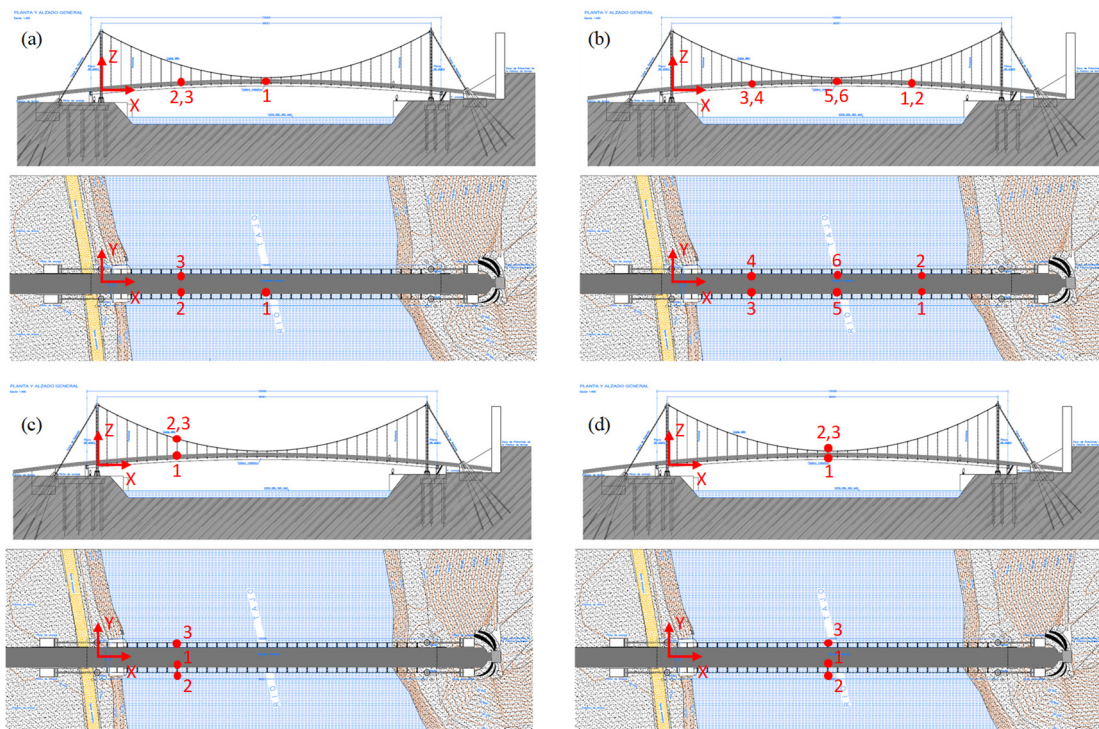


Fig. 5 Experimental layouts for the dynamic tests: (a) 02/03/2020, (b) 04/03/2020, (c) 03/03/2020, (d) 05/03/2020

on a possible dynamic coupling between the two subsystems. In the Fig. 5 have been illustrated the arrangements of the sensors used in the 4-days of experimental campaign using the six piezoelectric accelerometers. The setup disposed in the days 02 and 04 March (Figs. 4(a) and (b)) have been designed for identifying the frequencies of the deck. In particular, in the first one, the six sensors have been placed in three nodes (two accelerometers in each position) and in each one have been measured both the transversal (horizontal direction perpendicular to the bridge axis) and vertical component. Two sensors have been collocated in the middle span (point 1) while the other four in quarter of the length and in both side (points 2 and 3). Instead, in the second layout, the accelerometers have been placed in six different points of the deck and in each one has been recorded the vertical acceleration. The experimental layouts implemented in the days 03 and 04 March have been used to identify the modal parameters in the two main suspended cables (where for the sensors linked in the cable “transversal” and “vertical” mean the cable out-of-plane and in-plane accelerations). In particular, in the first case, all sensors have been placed at a quarter of the length with the aim to better catch the anti-symmetric modes. Instead, the second case (Fig. 4(d)) all sensors have been collocated in middle span, to better identify the symmetric modes. The maximum time of acquisition has been slightly different in each test but at least a total of 2400 s has been recorded using a sample time of 200 Hz.

The experimental layouts arranged using the six seismographs have been organized maintaining fixed two sensors on the upstream and downstream edges and varying the position of the other four. In this manner, have been taken into account 38 measurements points, indicated by red circles in Fig. 6, chosen to achieve an accurate

identification of the modal components (section 13 has been selected as reference). The accelerations have been acquired in continuous for a period of 18 minutes in each setup. A total of $18 \times 2 = 36$ measurements for each direction corresponding to the environmental noise response have been acquired. For this experimental test has been used a sample frequency of 100 Hz subsequently decimated to a range of 0-12.5 Hz. In Fig. 7 are reported four examples of time histories recorded by the piezoelectric accelerometers in both deck (Figs. 7(a) and (b)) and cable (Figs. 7(c) and (d)). Of course, due to their high lightness, it is easy to verify that the structural response under environmental noise, shown in the cables, is sensibly higher than the one exhibited by the deck. Moreover, while for the deck the vertical accelerations are higher than the corresponding transversal ones, it happens exactly the opposite in the cables. These observations have been numerically checked calculating the standard deviation for each time history where it is right to highlight that even the maximum value (recorded for transversal acceleration in the cable) assumes a very low amplitude ($1.0966e10^{-4}$).

3.3 Modal identification

The identification of modal parameters has been developed using well-known techniques as Enhanced Frequency Domain Decomposition (EFDD, Brincker *et al.* 2001), Stochastic Subspace Identification (SSI, Peeters and De Roeck 1999) and Polymax (Peeters and Van der Auweraer 2015). The first two procedures have been performed through the software Artemis while the third one by LMS TestLab.

Fig. 8(a) shows the singular values of the power spectra associated to the set of measurements performed using the seismographs. The peaks of such graph reveal the placement

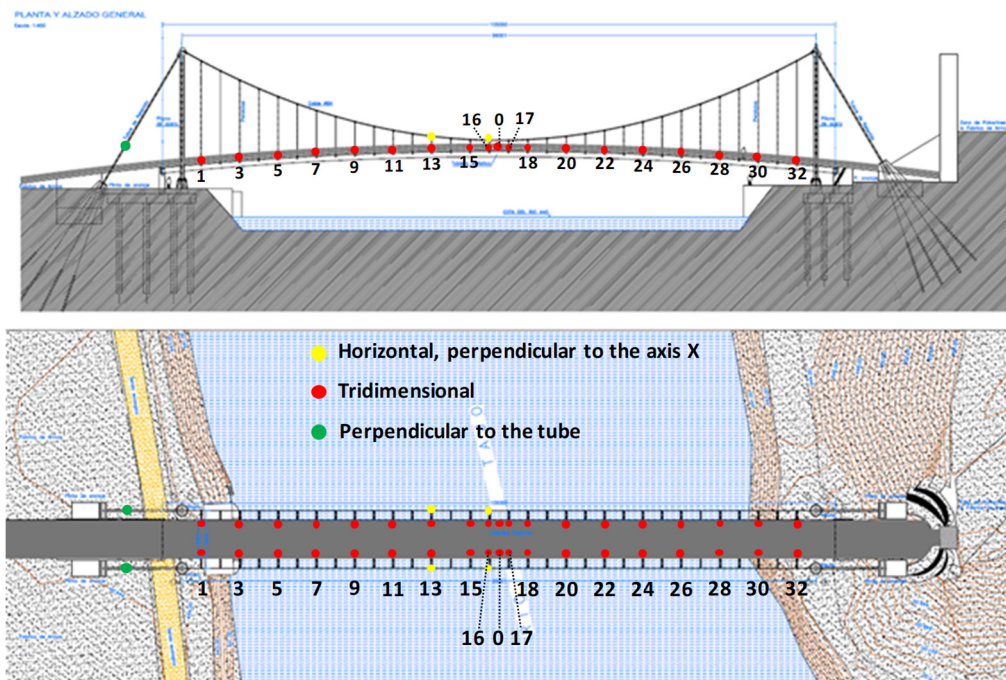


Fig. 6 Measurements points covered by the experimental layouts implemented using the six seismographs

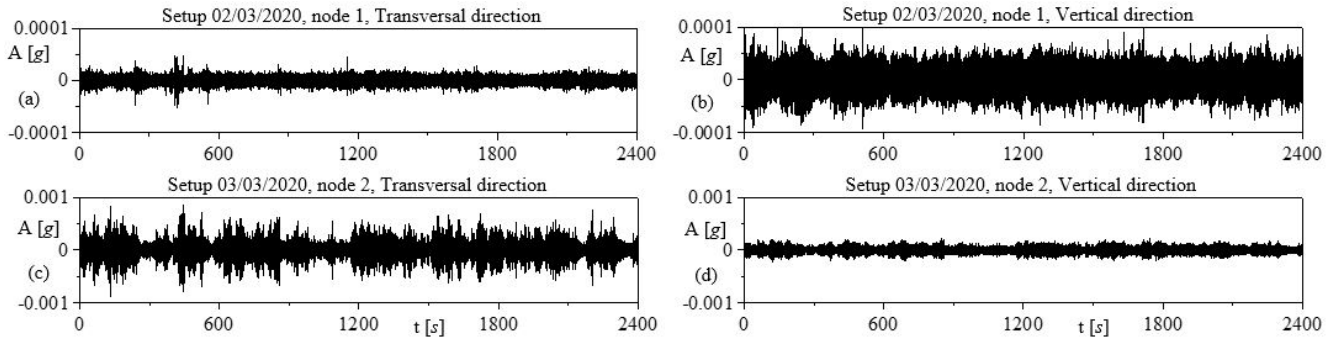


Fig. 7 Example of time histories recorded during the 4-days of experimental campaign

Table 3 Standard deviations of the accelerations depicted in Figure 7

	Deck		Cable	
	Transversal	Vertical	Transversal	Vertical
Standard deviation	$5.1154e10^{-6}$ g	$1.5806e10^{-5}$ g	$1.0966e10^{-4}$ g	$3.6021e10^{-5}$ g

of the structure natural frequencies. In order to distinguish the components of the vibration modes, power spectra of the accelerations collected at the reference section (number 13 in the Fig. 6) are shown in the Figs. 8(b) and 8(c) according to the Y-direction (transversal to the bridge longitudinal axis) and the vertical Z-direction. Some observations looking to these figures are the following: (1) they show independent peaks in the vertical and transversal direction, except for a few modes that probably include torsion and transversal components; (2) the first transversal vibration mode (well visible in Fig. 8(b)) has a relatively high damping level (wide peaks) with a frequency situated between the frequencies of the first two vertical modes; (3) the amplitude in the transversal direction is significantly smaller than that in the vertical direction. This latter observation was well visible also looking to the accelerations recorded by piezoelectric sensors (see Fig. 7) and explains the difficulty in identifying the modal configuration of the first transversal vibration mode.

The identified modes for the deck are reported in Table 4 and their perspective view is reported in Fig. 9. In particular, the modal shapes are referred to the vertical modes. The first one is collocated to a frequency of 0.755 Hz showing an anti-symmetric configuration. This is probably due to the fact that the first mode is driven by two main suspended cables. Indeed, such cables have a very high Irvine parameter $\lambda^2 = 897$, especially determined by a high sag of 14 m. Instead, the second and third ones are symmetric showing well separated frequencies that are respectively of 0.924 Hz and 1.585 Hz. The torsional modes are placement in higher frequencies, 3.263 Hz and 4.474 Hz. It is relevant to mention that although the structure is symmetric, vibration modes exhibit some asymmetry that is more evident for higher order modes. Moreover, there were some cases in which the level of the signal was too low for estimating the modal damping. For this reason, in some modes has been inserted “non-determined” in Table 4.

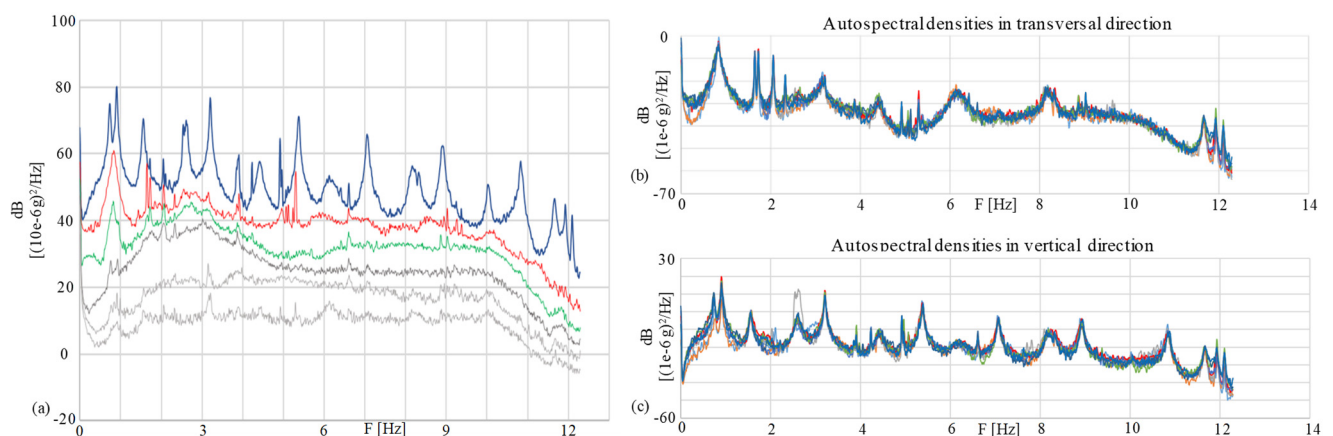


Fig. 8 (a) Singular values of the average power spectra (longitudinal, transversal and vertical directions); autospectral densities in transversal (b) and vertical (c) directions

Table 4 Main modes identified for the deck

Mode	Frequency [Hz]	Damping [%]	Shape
1	0.755	2.229	1 st Anti-symmetric vertical
2	0.870	Non-determined	1 st Transversal
3	0.924	1.483	1 st Symmetric vertical
4	1.585	1.453	2 nd Symmetric vertical
5	2.087	Non-determined	2 nd Transversal
6	2.639	1.608	2 nd Anti-symmetric vertical
7	3.263	0.403	1 st Symmetric torsional
8	3.979	Non-determined	3 rd Symmetric vertical
9	4.474	1.174	2 nd Anti-symmetric torsional
10	6.277	0.134	2 nd Symmetric torsional

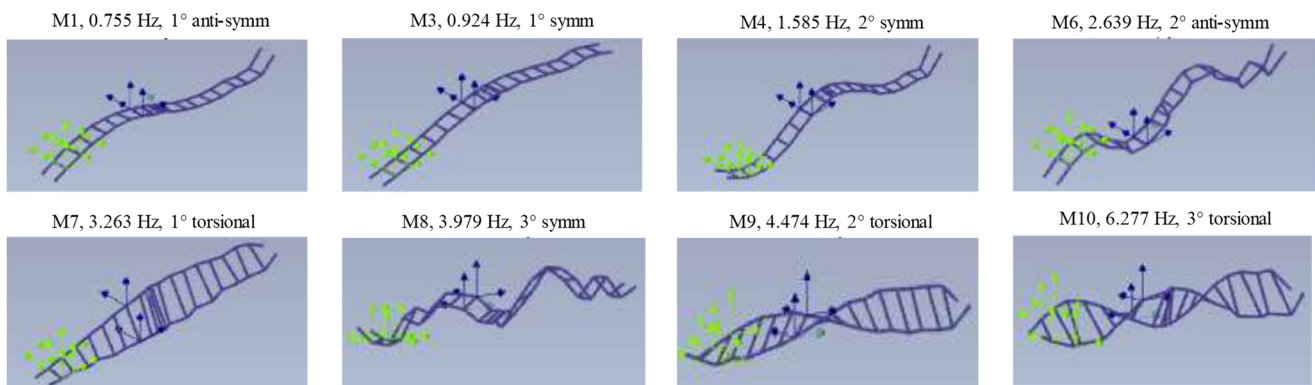


Fig. 9 Main modal shapes identified in vertical direction for the deck

It is thought that this asymmetry is related to a constraint to motion of the bridge by branches of trees located close to the hanger identified in section 30 (Fig. 6). Fig. 4(d) illustrates this aspect. The observation illustrated before are supported also by the data processing carried out on the measurements recorded by piezoelectric sensors. In particular, in the Fig. 10, have been reported the results analyzing the time histories obtained in the days 02/03/2020 (experimental layout of Fig. 5(a)) and 04/03/2020 (experimental layout of Fig. 5(b)). Moreover, it is right to underline that from the transversal measurements have not been captured modal signatures probably due to the low vibrational amplitude. For this reason, the identification results are all referred to the vertical direction. The stabilization diagrams, obtained through the Polymax procedure, have provided a good understanding of the main modal frequencies as shown in the Fig. 10(a). Nevertheless, such instrumentation has been able to identified only some modal shapes found by the experimental layouts arranged using the seismographs. This fact was mainly due for the following reasons: (1) few sensors available (only six that had to be disposed using coaxial cable); (2) main frequencies collocated under 1 Hz (difficult to be identified using piezoelectric technology); (3) dynamic tests performed under strong wind (in anyway same condition also for seismographs); (4) multiple frequencies associated with cable modes mixed with frequencies of the deck. In the Figs. 10(b) and 10(c) have been reported the Power Spectral

Densities (PSDs) calculated using measurements recorded in centerline (in black line) and at a quarter of the length (in red line) in both experimental setups. Substantially, the modes identified have been the following: the first (setup in Fig. 5(a)) and third symmetric (setup in Fig. 5(b)) modes collocated at 0.928 Hz and 3.979 Hz, the first torsional mode (setup in Fig. 5(b)) at 3.271 Hz. Such modal shapes have been also illustrated in the second row of Fig. 10. It is easy to appreciate, through a rapid visual comparison, that the modal deformations are in a good agreement with the corresponding ones found processing the signals recorded by seismographs.

In order to understand the dynamic behaviour of the main cables and their coupling with the deck, different experimental tests have been performed under environmental noise attaching the sensors simultaneously to the cables and the deck. This has been possible thanks to the help of professional climbers. In the Figs. 11(a) and 11(b) have been reported the PSDs calculated using the measurements recorded in two main cables. Moreover, the transversal accelerations (Y-direction in Figs. 5(c) and 5(d)) have been captured in the centerline and in the section placed to a quarter of the total length. It should be noted that signals at the centerline and the ones at a quarter of the length have been acquired in two different tests. The data processing shows clearly what are the frequencies associated to the main transversal modes: 1.672 Hz, 1.746 Hz, 2.087 Hz and 2.368 Hz. The first two frequencies

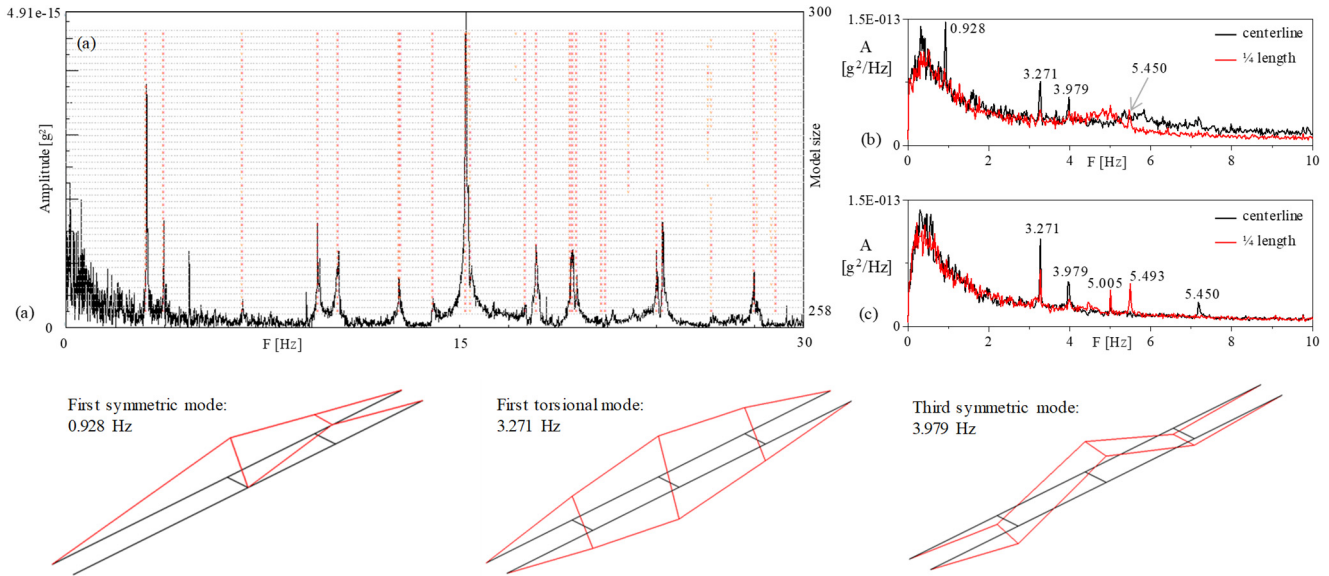


Fig. 10 Data processing of the data measured by piezoelectric sensors in the deck: (a) stability diagram obtained through Polymax; PSDs for (b) first setup (Figs. 5(a)) and (c) second setup (Fig. 5(b)); main modal shapes identified for the deck

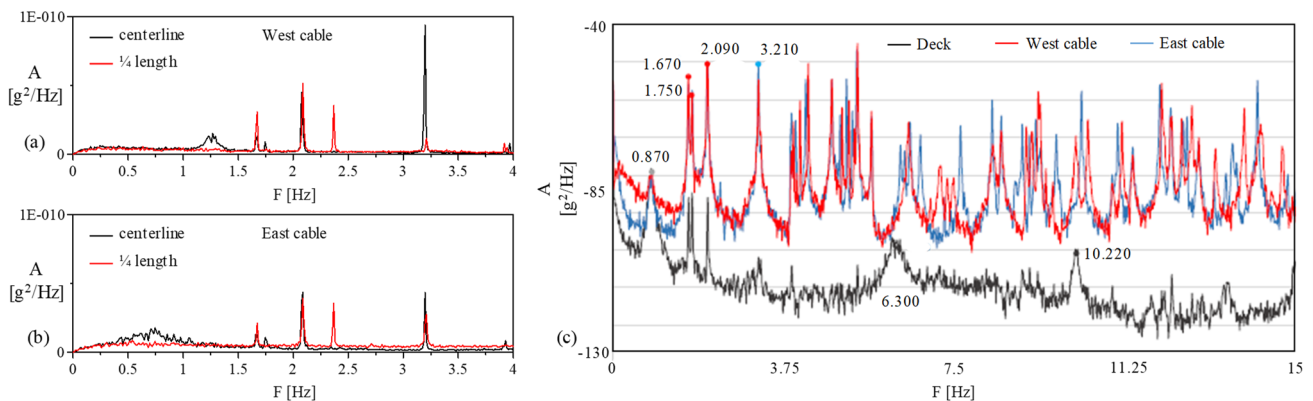


Fig. 11 (a), (b) PSDs measured in the two main cables in centerline and $\frac{1}{4}$ of the total length (Figs. 5(d) and (c)); (c) PSDs: comparison between deck and cable response (section 13 of the setup in Fig. 6). All results are related to the transversal direction.

correspond to the symmetric modes in which the cables are in phase and in opposition phase, respectively. The frequency 2.368 Hz is, instead, associable to an anti-symmetric mode because it appears in the measurement recorded in the section at a quarter while completely disappears in the one at the centerline. The results illustrated in the Fig. 11(c) are related to other test aim to investigate the coupling between the deck and cables. The tests have been carried out in centerline (section 16 in the setup of Fig. 6). Such figure shows a substantial independency between transversal deck and cables modes even if in some case a weak coupling is recognizable. Indeed, from these measurements, it is visible that in the frequency collocated to 0.870 Hz the deck and cables vibrate in phase with similar amplitude. Regarding the other frequencies (1.672, 1.746, 2.087, 2.368) it is, instead, well observable a remarkable difference between the levels of amplitude for cable and deck (much higher in the cables).

The modes at 6.300 Hz and 10.220 Hz, whose horizontal components are probably associable to the torsional modes, are poorly recognizable in the cables. The modal configurations have been analyzed looking to the amplitudes and phases of the frequency response functions relating accelerations at the deck and cables. The characteristics of the horizontal modes based on the modal components in cable and deck are reported in the Table 5. The vertical modes and components in the cable are the same as the ones in the deck.

A final set of dynamic tests have been conducted on the backstay cables that aimed at identifying the installed force using the so-called vibrating chord method (Figs. 12(a) and 12(b)). In reality, because the backstay cables are made of hollow tubes and are relatively short, bending effects may be relevant.

Therefore, instead of applying directly the vibration chord theory, the force evaluation was made on the basis of

Table 5 Modal transversal components identified at section 13

Frequency [Hz]	Modal components			Characteristics of the mode
	East cable	West cable	Deck	
0.870	1.000	1.010	0.989	Cables in phase and with deck
1.670	1.000	-0.573	-0.008	Cables in opposition of phase, East cable opposition phase to deck
1.750	1.000	0.260	-0.063	Cables in phase and in opposition of phase to deck
2.090	1.000	0.287	-0.006	Cables in phase and in opposition of phase to deck
2.360	1.000	-0.205	0.005	Anti-symmetric mode, cables in opposition of phase, East cable in phase with deck
3.230	1.000	0.598	-0.007	Cables in phase and in opposition of phase to deck
3.940	1.000	-0.125	-0.001	Cables in opposition of phase, East cable opposition phase to deck

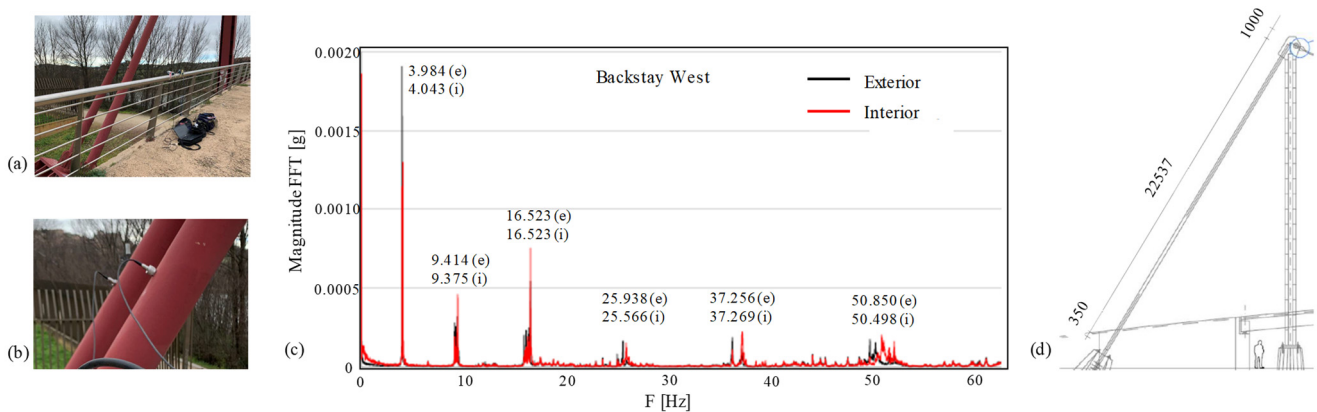


Fig. 12 (a), (b) Measurements in backstay cables; (c) magnitude of Fourier spectrum for the corresponding measurements; (d) sketch of the backstay model

the fitting of a finite element model considering the identified natural frequencies. The latter have been identified from measurements under environmental noise in these two backstay cables at a distance from the anchorage of about 2 m. Fig. 12(c) reports the average Fourier spectra of the accelerations measured on the two cables simultaneously. The identified frequency peaks are summarized in the Table 6. The evaluation of the force has been pursued through a numerical model (geometry sketched in Fig. 12(d)) in which the installed tension was iteratively adjusted in order to fit the natural frequencies measured. Identified and numerical frequencies are very close each other for the following values of the estimated forces: 1664 KN (exterior cable) and 1643 KN (interior cable).

Table 6 Identified frequencies for two backstay cables

Mode	Exterior cable [Hz]	Interior cable [Hz]	Numerical model [Hz]
1	3.984	4.043	4.082
2	9.414	9.375	9.378
3	16.523	16.523	16.521
4	25.938	25.566	25.697
5	37.256	36.269	36.958
6	50.850	50.498	50.300

4. Model updating

The structural models are in general implemented and formulated to describe their behavior under different type of excitations. Such models depend on different parameters used to represent the material properties, soil-structure interaction or types of constrains. These parameters could be affected by a series of uncertainties that could be reduced by the information coming by experimental tests. In the literature different strategies developed for the models updating can be found as the ones reported in Jafarkhani and Masri (2011) and Mottershead *et al.* (2011). The following section reports the results related to the analytical and numerical models representative of the structural behavior for Polvorines walkway.

4.1 Analytical model

The Differential Evolution (DE) method, first proposed by Storn and Price (1997), is adopted to perform the identification of the parametric system and characterize the modal features of the suspension bridge. The aim is to find feasible mechanical parameters of the bridge model that allow to reproduce accurately the frequencies and mode shapes identified experimentally.

The approach consists of generating a set of n parameters vectors from uniform probability distributions to ensure that the parameters span the space equally and respect the constraints. The eigenvalue problem associated

with the equations of motion describing the free, undamped oscillations of the bridge was solved for each set of vectors, and the lowest frequencies of the bridge mode shapes were calculated for each simulation. The DE algorithm then perturbs a randomly selected vector chosen from among $n-1$ vectors of the first generation and provides a new mutated parameters vector (i.e., a trial vector); frequencies and mode shapes are then calculated for the generated trial parameters vector and a cost function F^{tri} is calculated and compared with the objective function F^{tar} evaluated for the parameters vector (namely, the target vector) excluded in the generation of the trial vector. If $F^{tri} < F^{tar}$, the trial vector survives; otherwise, the target vector is selected for creating the new generation of parameters vectors which best perform in terms of control. The algorithm proceeds by providing new generations of parameters vectors up to the achievement of the minimum value of the objective function.

The steps adopted in the identification procedure can be summarized as follows:

- (1) Target functions are first introduced as the discrete vectors of the experimentally identified frequencies of the vertical, the torsional and the lateral motion of the suspension bridge, respectively. In particular, $f_v = [0.755, 0.924, 1.585, 2.639]$ Hz and $f_\phi = [3.263, 4.474, 6.277, 8.341]$ Hz are the vectors of the lowest four frequencies calculated for the vertical and the torsional motion of the deck, respectively, while, $f_w = [0.870]$ Hz and $f_u = [0.870]$ Hz are the vectors of the lowest frequencies of the lateral motion of the deck and the cables, respectively. On the other hand, the mode shapes corresponding to each frequency experimentally identified and collected in the above mentioned vectors are listed in the following vectors: $S_v = [2,1,3,4]$, $S_\phi = [1,2,3,4]$, $S_w = [1]$, $S_u = [1]$, respectively. In the latter expressions, numbers 1, 2, 3, and 4 were adopted to identify the first symmetric, the first anti-symmetric, the second symmetric, and the second anti-symmetric mode shape, respectively. According to the geometric parameters provided by the technical drawings of the suspension bridge here investigated (i.e., $l = 99$ m and $f_0 = 14$ m), the following value of the parameter g was found: $g = 1.1031$. Moreover, since the identification procedure was applied to the nondimensional mechanical parameters of the bridge, the deck mass per unit length mD, adopted in the nondimensionalization, was not identified, and set equal to $mD = 2500$ kg/m according to the data available from the technical drawings. Finally, the characteristic frequency turned out to be $w_c = 0.15177$ 1/s.
- (2) A trial range of variation of the parameters κ_v , κ_w , κ_ϕ , κ_c , μ , and J_μ , respectively, is assigned starting from the tentative values κ_v^0 , κ_w^0 , κ_ϕ^0 , κ_c^0 , μ^0 and J_μ^0 , (i.e., extracted from the design parameters of the bridge). In particular, since the cables mechanical parameters κ_c^0 and μ^0 are the less uncertain, those were varied in a range of

$0.50 \leq \kappa_c/\kappa_c^0 \leq 2.00$ and $0.75 \leq \mu/\mu^0 \leq 1.25$, while the resulting parameters were varied in the range $[0.1, 10]$ times their reference value.

- (3) In the first iteration, the eigenvalues and the corresponding shapes of the lowest modes of the bridge were calculated for an initial population of parameters (i.e., $n = 50 \times Np$ vectors, where the number of parameters to be identified is here equal to $Np = 6$).
- (4) The cost functions $F1i$ are evaluated as the Mean Square Error of the difference vectors between the reference (experimental) and the numerical frequencies, for i th unknown (i.e., $F1v$, $F1\phi$, $F1w$, $F1u$); while, the cost function $F2i$ is evaluated as the Mean Square Error of the difference vectors between the reference vectors S_v , S_ϕ , S_w , and S_u and the numerically calculated vectors providing the modal sequence (i.e., $F2v$, $F2\phi$, $F2w$, $F2u$). Therefore, the weighted cost function

$$F = c_{11}F1v + c_{12}F1\phi + c_{13}F1w + c_{14}F1u + c_2(F2v + F2\phi + F2w + F2u) \quad (8)$$

is evaluated by adopting as weighting coefficients $c_{11} = 10$, $c_{12} = 10$, $c_{13} = 1$, $c_{14} = 1$ and $c_2 = 10$, respectively. The criterion of selection of such weighting coefficients has been driven by the idea of forcing the algorithm to weight more the discrepancy between experimental and numerical frequency of the vertical and the torsional mode of the bridge (the most important and also those for which we have more frequencies identified) and to give less importance to the identification of the frequencies referred to the lateral motion (of the deck and of the cable).

- (5) Further iterations were then performed for the minimization of the cost function F by combining and mutating the populations of parameters according to the DE algorithm so as to move towards improved generations of parameters (i.e., leading to a minimum cost function F_{min}). In particular, $Ng = 250$ generations of parameters populations were generated to reach a suitable asymptotic behavior of the cost function.

The computational time for each iteration ($50 \times 6 = 300$ populations), performed within parallel computing of 6 cores, was about 5 seconds, while the total computational time over 250 generations of 300 populations was about 18 minutes. Table 7 summarises the initial and optimized parameters obtained by this procedure. In the third row of this table, the ratios between the optimized parameters and the initial values are presented. As expected, the differences are very large putting in evidence the difficulty in the estimation of the parameters for this type of modelling. Large uncertainty emerged concerning the evaluation of the rotational mass, the vertical bending stiffness, and the torsional stiffness of the bridge deck. This could be due to a rough evaluation of the initial, tentative value assumed for the three parameters. Those were calculated by evaluating displacements and rotations for given loading conditions

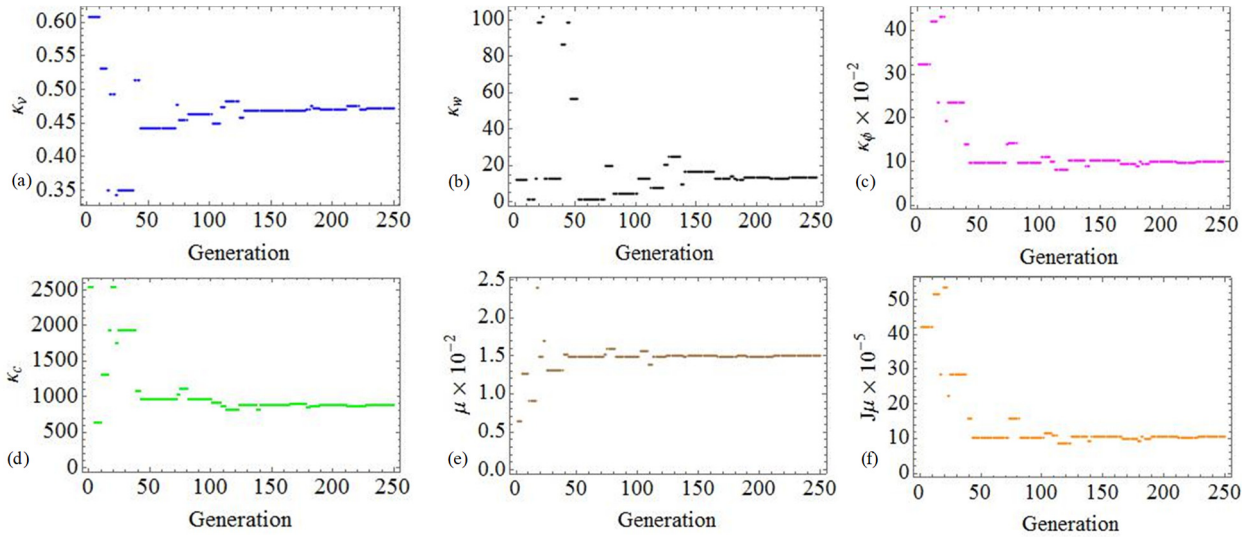


Fig. 13 Nondimensional parameters corresponding to the optimal population of each generation

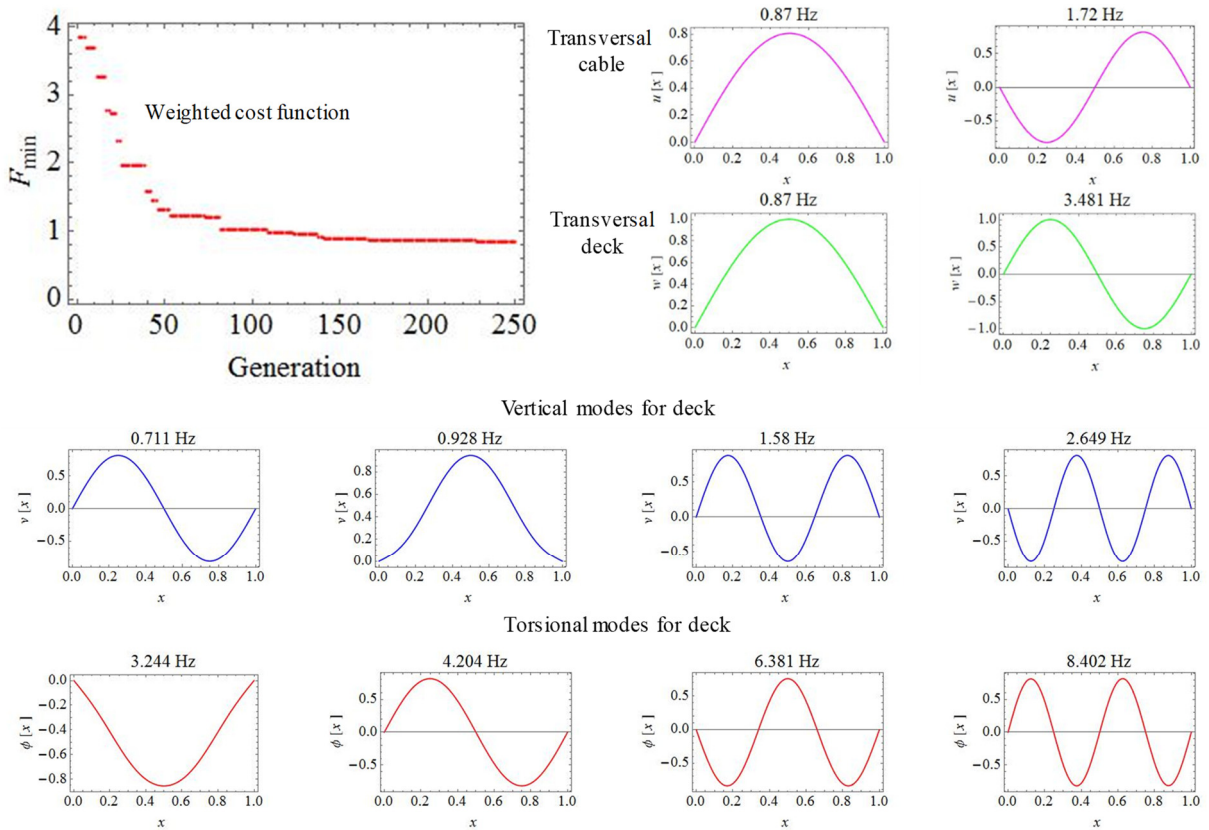


Fig. 14 Weighted cost function varying the number of generations and modal shapes related to the optimal solution

using a FE model of the bridge deck. The evaluated displacements and rotations were then used to calculate the bending and the torsional stiffnesses, respectively, using the exact solution of the corresponding elastic problem obtained by means of the analytical model of a one-dimensional beam subjected to the same boundary conditions of the deck. Finally, the rotational mass was calculated by means of the radius of gyration derived from the polar moment of inertia estimated for the deck cross-section. In the Figs. 13 and 14 are illustrated the variations

of the structural parameters with the generation model number and the modal shapes calculated for the optimized system. Such modal shapes show to be perfectly correlated with the identified ones and also difference between the experimental and analytical frequencies are very low as well observable in Table 8. In Fig. 12 are shown the values of the nondimensional identified parameters corresponding to the optimal population of each generation, that are the parameters for which the lowest value of the objective function (i.e., F_{min}) is reached.

Table 7 Tentative nondimensional parameters, optimized nondimensional parameters and their ratio

μ^0	κ_c^0	κ_v^0	κ_w^0	J_μ^0	κ_ϕ^0
0.0172	1387.37	1	14.716	5.351×10^{-5}	0.4188
μ	κ_c	κ_v	κ_w	J_μ	κ_ϕ
0.0149	871.93	0.472	13.327	1.050×10^{-4}	0.099
μ/μ^0	κ_c/κ_c^0	κ_v/κ_v^0	κ_w/κ_w^0	J_μ/J_μ^0	$\kappa_\phi/\kappa_\phi^0$
0.871	0.628	0.472	0.906	1.962	0.236
Cable mass [kg/m]	Cable axial stiffness [N]	Deck vert. flex. stiffness [Nm ²]	Deck hor. flex. stiffness [Nm ²]	Deck rotational mass [kg m ² /m]	Deck torsional stiffness [Nm ²]
37.451	4.921×10^8	2.611×10^9	7.372×10^{10}	2572.03	5.469×10^8

Table 8 Comparison between experimental and optimized frequencies of the analytical model (AM)

Mode	Exp. Frequency [Hz]	AM. Frequency [Hz]	Difference (%)
1 st vertical deck	0.755	0.711	-5.83
1 st transversal deck	0.870	0.870	0.00
1 st transversal cable	0.870	0.870	0.00
2 nd vertical deck	0.924	0.928	0.43
3 rd vertical deck	1.585	1.580	-0.32
2 st transversal cable	1.750	1.720	-1.71
4 th vertical deck	2.639	2.649	0.37
1 st torsional deck	3.263	3.244	-0.58
2 st transversal deck	Not identified	3.481	-
2 nd torsional deck	4.474	4.204	-6.04
3 rd torsional deck	6.277	6.381	1.66
4 th torsional deck	8.341	8.402	0.73

4.2 Numerical model

The walkway Polvorines has also been modelled through a numerical finite element model realized in the environment of the software MIDAS Civil (Fig. 15(a)). The geometry of the model faithful respects the one of the construction drawings. The geometrical information has been accurately selected even thanks to the realization of a BIM model (Figs. 15(e) and 15(f)) constructed with images acquired by UAV used to derive a 3D point cloud model. The boundary conditions have been applied to the end of the four pylon and backstay cables but also at the end of the deck. In particular, while in the first two cases all possible degree of freedom has been restrained, in the case of the deck has been realized a modeling detail illustrated in Fig. 15(b) corresponding to the real arrangement of Fig. 15(c). In particular, in the node 1 (Fig. 15(b)) all the rotations have been left free while all the displacements have been fixed. In the nodes 2 and 3 (Fig 15(b)) the only free degree of freedom is the one in vertical direction that has been constrained applying a vertical linear elastic spring. This last choice aims to comply, as first hypothesis, to the constructive detail shown in Figs. 3(d) and 3(e). The two main cables and the hangers have been modelled through a finite element available in the library of Midas Civil called “*Tension only, Hook, Cable*”. Two full circular sections with diameter of 84 mm and 16 mm have been adopted

respectively for the main cables and the hangers. Instead, the deck has been represented by a beam for which has been used a single-celled box with a collaborating concrete slab (thickness of 20 cm). A further detail of the link beam-hanger is reported in the Fig. 15(d). In this case this element has been modelled, using a small beam, even to taken into account its mass.

Such section has been implemented within the typology *Steel-Tube Type 1* that allowed to realize a mixed steel-concrete section. In this case, moreover, have been inserted also the initial values for the ratio between the elastic moduli of steel and concrete, $a = E_s/E_c$, and the ratio between the specific weights of steel and concrete, $r = D_s/D_c$, fixed initially to 7 and 3 respectively. The four pylons, modelled by beams, possess a squared box section with side of 90 cm and thickness of 25 mm. Moreover, for each pylon has been provided a backstay tendon with a hollow circular section (diameter of 219 mm and thickness of 20 mm). It is highlighted that in the real case there are two backstay tendons for each pylon but for simplicity only one element has been used. Finally, the one-dimensional stiffening lateral elements of the deck have been modelled using beams with an average section of IPE450. The steel material has been, at first, selected with the following characteristics: elastic modulus $E_s = 180000 \text{ N/mm}^2$, specific weight $D_s = 78500 \text{ N/mm}^3$ and Poisson coefficient $n = 0.3$. In the numerical model the characteristics of the concrete

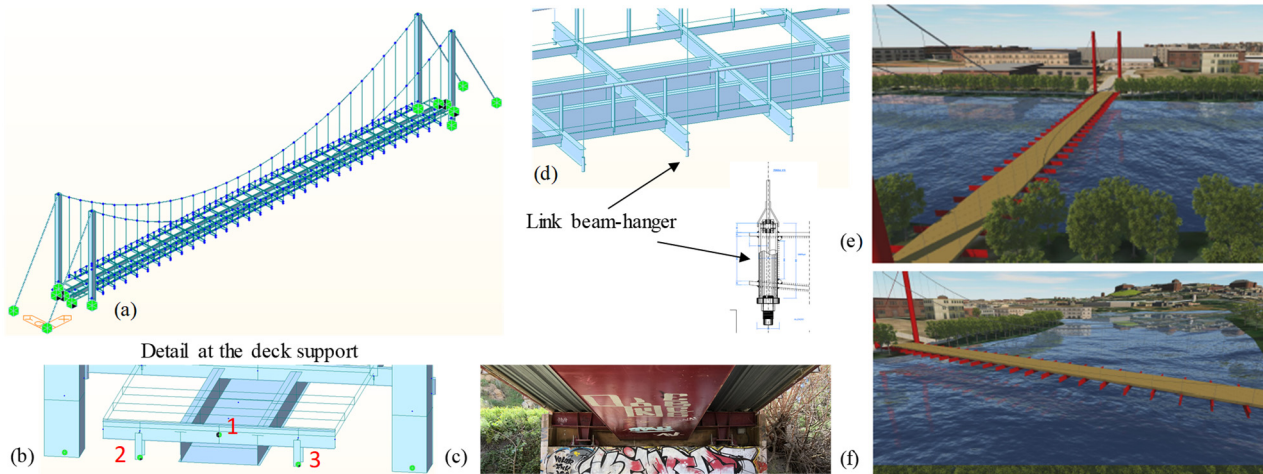


Fig. 15 Finite element model of the walkway Polvorines (a). Modeling details for deck support (b) with photo of the its real arrangement (c) and link beam-hanger (d). Images of the BIM model (e), (f)

Table 9 Comparison between experimental and numerical frequencies in the main global modes

Mode number in FEM	Experimental frequency [Hz]	Numerical frequency [Hz]	Difference (%)	Modal shape
1	0.755	0.713	-5.56	1 st antisym. vertical
2	0.870	0.835	-4.02	1 st sym. transversal
3	0.924	0.904	-2.16	1 st sym. vertical
6	1.585	1.579	-0.38	2 nd sym. vertical
12	2.639	2.633	-0.23	2 nd antisym. Vertical
16	3.263	3.283	0.61	1 st torsional (deck driven)
23	3.979	4.010	0.78	3 rd sym. vertical
26	4.474	4.374	-2.24	2 nd torsional

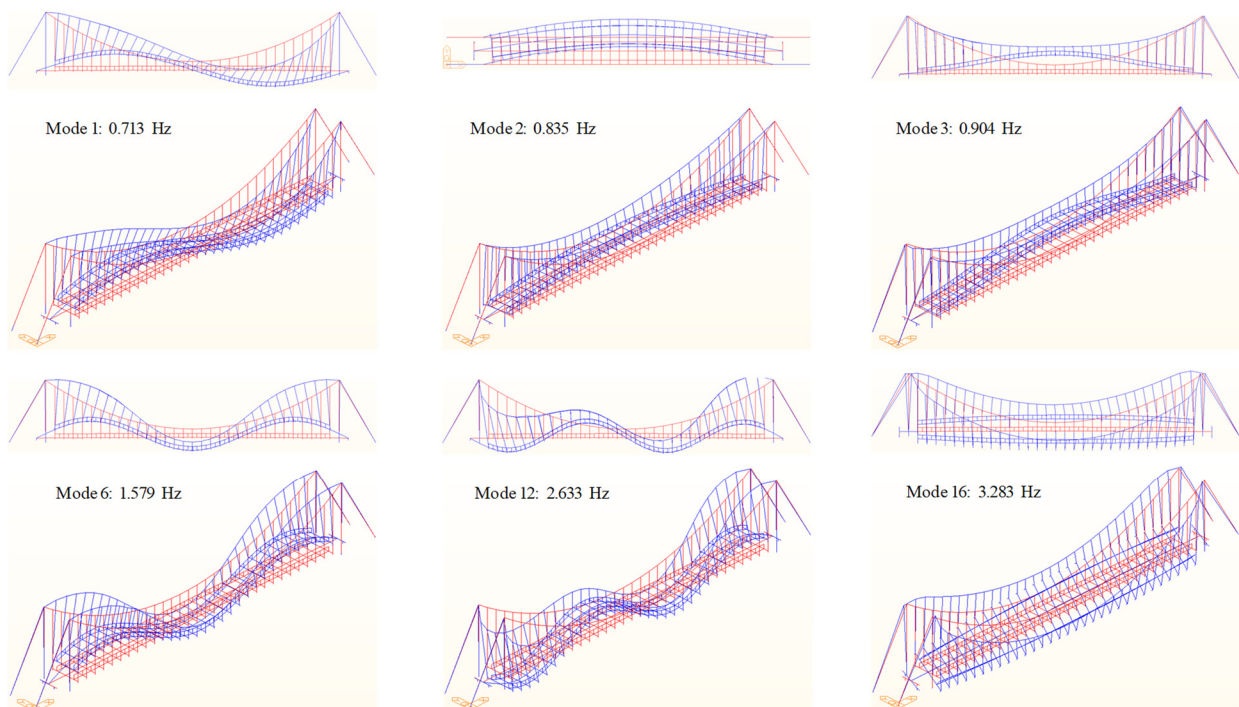


Fig. 16 Six modal shapes of the updated finite element model matching identified global modes

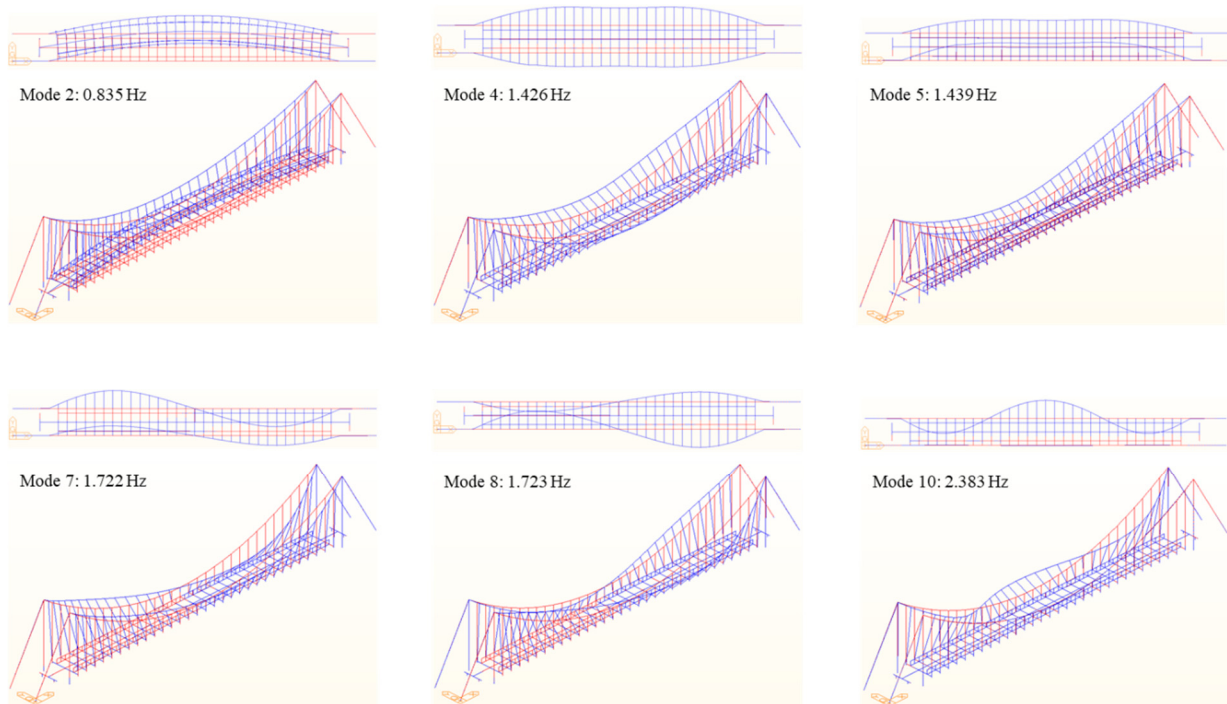


Fig. 17 Modes in the finite element model involving the cables in the transversal motion

Table 10 Comparison between experimental and numerical frequencies in modes involving the cables in transversal motion

Mode number in FEM	Experimental frequency [Hz]	Numerical frequency [Hz]	Difference (%)	Modal shape
2	0.870	0.835	-4.02	Cables in phase and with deck
4	1.670	1.426	-14.71	Cables in opposition of phase, East cable opposition phase to deck
5	1.750	1.439	-17.77	Cables in phase and in opposition of phase to deck

material is defined automatically by the ratios previously introduced.

The updating of the numerical model has been pursued minimizing the following function

$$\min \left(\sum_{i=1}^3 (f_{exp,i} - f_{num,i}) \right) \quad (7)$$

Such expression aims to minimize the sum of the first three differences between the experimentally identified frequencies and the numerical ones. The solution has been found changing a series of characteristics of the model both in the parameters and in the description of some details. In particular, to reach a reasonable matching of the vertical modes the steel Young modulus has been increased up to the value $E_s = 210000 \text{ N/mm}^2$ and the previously introduced a and r has retained very close to the initial values ($a = 7$ and $r = 3.1$). Instead to minimize the error for the symmetric torsional frequency has been considered useful to introduce in the model the parapet especially for its contribution to the torsional inertia. In the Table 9 is reported a comparison between the experimental and numerical frequencies for some relevant modes of which

the shape is qualitatively described in the last column of the table. For these modes an excellent matching has been reached. Instead, in the Fig. 16 have been shown the modal shapes for six modes that by a simple visual comparison perfectly comply the identified ones.

The mode 1, 3 and 6 are determined mainly by the first three in-plane modes of the suspended cable which has surely been resulted at spatial frequencies larger than the one characterizing the so-called crossover in the Irvine diagram. Indeed, the sequence involves both deck and cables in their plane with first an antisymmetric mode and then two symmetric modes. Furthermore, a deeper analysis of the modal shapes predicted by the FEM model permits to evaluate the sequence of modes involving mainly the suspended cable in the out-of-plane motion (see Fig. 17). Due to the few measurements obtained in the cable it has not been possible to define exactly the modal shapes of the cables in their spatial distribution. However, in Table 10 is presented a tentative trial of comparison and the sequence of modes depicted in Fig. 10 explain the complexity of local cable transversal motion which is confirmed by the numerous peaks of Fig. 11(c).

5. Conclusions

The paper offers relevant results in the knowledge of the dynamics of suspension cable bridge highlighting the reciprocal role of main cables and deck in both vertical and horizontal oscillations. Modeling and acquired data permits to rely on a clear representation of the mechanical behavior of the studied system. An important experimental campaign carried out on the walkway Polvorines enabled to identify the most important and relevant oscillation modes involving the vibration of the deck, the interaction between main cable and structures and the estimation of the backstays tendons. Moreover, such experience highlights how a more refined identification needs of both a widespread number of sensors on the deck and a simultaneous measure on deck and cables. Subsequently, appropriate methods have been applied to update the structural behavior of the walkway represented by both analytical and numerical models. The usefulness of such models is well recognizable in literature. Indeed, while the conciseness of the analytical model permits to analyses and better understand nonlinear and local internal mechanism, the numerical finite element models allows a better description of the geometry taking into account its effects on the dynamics with a consequent richness of the number of predicted modes. The simplifying hypothesis of the analytical model draw our attention on the main modes of the system, however the number of degree-of-freedom of the FEM model showed numerous modes which have not always found a counterpart in the identified modes obtained by the measurements and in the ones predicted by the analytical modes. As in previous experience conducted for a cable-stayed bridge (Caetano *et al.* 2008) the representation by a rich finite element model of the actual measurements obtained on the bridge remains a heavy task especially for modes involving mainly the relative motion of the cables. Dynamics of cable structures continues to show interesting phenomena even in the linear range.

Acknowledgments

Part of the research leading to these results has received funding from the Italian Government under Cipe resolution n.135 (Dec. 21. 2012) under the project INCIPICT-*Innovating City Planning through Information and Communication Technologies*.

The experimental results of the Polvorines steel bridge is part of the research project DESDEMONA - *DEtection of Steel Defects by Enhanced MONitoring and Automated procedure for self-inspection and maintenance* (grant agreement number RFCS-2018_800687) supported by EU Call RFCS-2017.

References

Antonacci, E., De Stefano, A., Gattulli, V., Lepidi, M. and Matta, E. (2012), "Comparative study of vibration-based parametric identification techniques for a three-dimensional frame structure", *J. Struct. Control Health Monitor.*, **19**(5), 579-608.

- <https://doi.org/10.1002/stc.449>
- Arena, A. and Lacarbonara, W. (2012), "Nonlinear parametric modeling of suspension bridges under aeroelastic forces: torsional divergence and flutter", *Nonlinear Dyn.*, **70**(4), 2487-2510. <https://doi.org/10.1007/s11071-012-0636-3>
- Arena, A., Lacarbonara, W. and Marzocca, P. (2016), "Post-critical behavior of suspension bridges under nonlinear aerodynamic loading", *J. Computat. Nonlinear Dyn.*, **11**(1), 011005, 1-11. <https://doi.org/10.1115/1.4030040>
- Brincker, R., Zhang, L. and Andersen, P. (2001), "Modal identification of output-only systems using frequency domain decomposition", *Smart Mater. Struct.*, **10**(3), 441-445. <https://doi.org/10.1088/0964-1726/10/3/303>
- Caetano, E., Cunha, A. and Taylor, C.A. (2000), "Investigation of dynamic cable-deck interaction in a physical model of a cable stayed bridge, Part I: Modal analysis", *Earthq. Eng. Struct. Dyn.*, **29**(4), 481-498. [https://doi.org/10.1002/\(SICI\)1096-9845\(200004\)29:4<481::AID-EQE918>3.0.CO;2-1](https://doi.org/10.1002/(SICI)1096-9845(200004)29:4<481::AID-EQE918>3.0.CO;2-1)
- Caetano, E., Cunha, A., Gattulli, V. and Lepidi, M. (2008), "Cable-deck dynamic interactions at the International Gadiana Bridge: On-site measurements and finite element modelling", *Struct. Control Health Monitor.*, **15**(3), 237-264. <https://doi.org/10.1002/stc.241>
- Casalotti, A., Arena, A. and Lacarbonara, W. (2014), "Mitigation of post-flutter oscillations in suspension bridges by hysteretic tuned mass dampers", *Eng. Struct.*, **69**, 62-71. <https://doi.org/10.1016/j.engstruct.2014.03.001>
- Cunha, A., Caetano, E., Magalhaes, F. and Moutinho, C. (2018), "Dynamic identification and continuous dynamic monitoring of bridge: different applications along bridge life cycle", *Struct. Infrastruct. Eng.*, **14**(3), 445-467. <https://doi.org/10.1080/15732479.2017.1406959>
- Gattulli, V. and Lepidi, M. (2007), "Localization and veering in the dynamics of cable-stayed bridges", *Comput. Struct.*, **85**(21-22), 1661-1678. <https://doi.org/10.1016/j.compstruc.2007.02.016>
- Gattulli, V., Lofrano, E., Paolone, A. and Potenza, F. (2019a), "Measured properties of structural damping in railway bridge", *J. Civil Struct. Health Monitor.*, **9**(5), 639-653. <https://doi.org/10.1007/s13349-019-00358-3>
- Gattulli, V., Lepidi, M., Potenza, F. and Di Sabatino, U. (2019b), "Modal interactions in the nonlinear dynamics of a Beam-Cable-Beam", *Nonlinear Dynamics*, **96**(4), 2547-2566. <https://doi.org/10.1007/s11071-019-04940-8>
- Gattulli, V., Lepidi, M., Potenza, F. and Di Sabatino, U. (2016), "Dynamics of masonry walls connected by vibrating cable in a historic structure", *Meccanica*, **51**(11), 2813-2826. <https://doi.org/10.1007/s11012-016-0509-9>
- Hu, W.-H., Moutinho, C., Caetano, E., Magalhaes, F. and Cunha, A. (2012), "Continuous dynamic monitoring of a lively footbridge for serviceability assessment and damage detection", *Mech. Syst. Signal Process.*, **33**, 38-55. <https://doi.org/10.1016/j.ymssp.2012.05.012>
- Hua, X., Wang, C., Li, S. and Chen, Z. (2020), "Experimental investigation of wind-induced vibrations of main cables for suspension bridge in construction phases", *J. Fluid Struct.*, **93**, 102846. <https://doi.org/10.1016/j.jfluidstructs.2019.102846>
- Irvine, H.M. (1981), *Cable Structures*, The MIT Press.
- Jafarkhani, R. and Masri, S.F. (2011), "Finite element model updating using evolutionary strategy for damage detection", *Comput.-Aided Civil Infrastruct. Eng.*, **26**, 207-224. <https://doi.org/10.1111/j.1467-8667.2010.00687.x>
- Jimenez-Alonso, J.F., Saez, A., Caetano, E. and Cunha, A. (2019), "Lateral crowd-structure interaction model to analyse the change of the modal properties of footbridges", *Struct. Control Health Monitor.*, **26**(6), e2356. <https://doi.org/10.1002/stc.2356>

- Koo, K.Y., Brownjohn, J.M.W., List, D.I. and Cole, R. (2013), "Structural health monitoring of the Tamar suspension bridge", *Struct. Control Health Monitor.*, **20**, 609-625.
<https://doi.org/10.1002/stc.1481>
- Larsen, A. and Larose, G.L. (2015), "Dynamic wind effects on suspension and cable-stayed bridge", *J. Sound Vib.*, **334**, 2-28.
<https://doi.org/10.1016/j.jsv.2014.06.009>
- Mao, J.-X., Wang, H., Xun, Z.-X. and Zou, Z.-Q. (2017), "Variability analysis on modal parameters of Runyang Bridge during Typhoon Masta", *Smart Struct. Syst., Int. J.*, **19**(6), 653-663. <https://doi.org/10.12989/sss.2017.19.6.653>
- Mottershead, J.E., Link, M. and Friswell, I. (2011), "The sensitivity method in finite element updating: A tutorial", *Mech. Syst. Signal Process.*, **25**, 2275-2296.
<https://doi.org/10.1016/j.ymsp.2010.10.012>
- Nie, Z., Guo, E., Li, J., Hao, H., Ma, H. and Jiang, H. (2020), "Bridge condition monitoring using fixed moving principal component analysis", *Struct. Control Health Monitor.*, **27**, e2535. <https://doi.org/10.1002/stc.2535>
- Peeters, B. and De Roeck, G. (1999), "Reference-based stochastic subspace identification for output-only modal analysis", *Mech. Signal Signal Process.*, **13**(6), 855-878.
<https://doi.org/10.1006/mssp.1999.1249>
- Peeters, B. and Van der Auweraer, H. (2015), "Polymax: a revolution in operational modal analysis", *Proceedings of the 1st Operational Model Analysis Conference*, Copenhagen, Denmark, April.
- Siringoringo, D.M. and Fujino, Y. (2018), "Seismic response of a suspension bridge: Insights from long-term full-scale seismic monitoring system", *Struct. Control Health Monitor.*, **25**(11), e2252. <https://doi.org/10.1002/stc.2252>
- Storn, R. and Price, K. (1997), "Differential Evolution – A simple and efficient heuristic for global optimization over continuous spaces", *J. Global Optimiz.*, **11**, 341-359.
<https://doi.org/10.1023/A:1008202821328>
- Wickramasinghe, W.R., Thambiratnam, D.P. and Chan, T. (2020), "Damage detection in a suspension bridge using modal flexibility method", *Eng. Fail. Anal.*, **107**, 104194.
<https://doi.org/10.1016/j.engfailanal.2019.104194>
- Zhou, H.F., Ni, Y.Q. and Ko, J.M. (2013), "Structural health monitoring of the Jiangyin Bridge: System upgrade and data analysis", *Smart Struct. Syst., Int. J.*, **11**(6), 637-662.
<https://doi.org/10.12989/sss.2013.11.6.637>